Geophys. J. Int. (1998) **132,** 595–602

A Maslov–Kirchhoff seismogram method

X. Huang,[1] G. F. West[1] and J.-M. Kendall[2]
[1] *Department of Physics, University of Toronto, Toronto, Ontario, Canada* M5S 1A7
[2] *Department of Earth Sciences, University of Leeds, Leeds,* LS2 9JT, *UK*

Accepted 1997 September 2. Received 1997 August 4; in original form 1996 December 19

SUMMARY

When synthetic seismograms are computed for complicated velocity models using asymptotic methods based on ray theory, the caustic and/or pseudo-caustic geometrical catastrophes that often occur in the ray manifolds can cause many difficulties, because ray amplitudes can become infinite, inaccurate or vanish in such situations. The longer the propagation path relative to the scale of the velocity inhomogeneities and the more the propagation tends to be oblique rather than normal to velocity variations, the more troublesome the catastrophes become.

Although the Maslov integral method (MI) largely cures the problems of the classical geometric ray theory (GRT) at caustics (where nearby rays in geometrical space cross) and in geometric shadow zones, it suffers from serious artefacts at pseudo-caustics (the crossing points of rays drawn in the mixed geometrical and slowness space of the Maslov integral). Some methods have been devised to overcome this limitation, but none is satisfactory when it is necessary to compute automatically large suites of seismograms for complex models without continuous intervention from a skilled seismologist.

In this paper, we demonstrate how combining the Maslov integral method with a stage of Kirchhoff integration can greatly reduce MI's pseudocaustic problems while retaining MI's ability to overcome the caustic and shadow problems of GRT. In many cases, the additional computational burden increases by one order of magnitude but is still much less than that required in a finite-difference modelling, and is not great for a common workstation. The Maslov–Kirchhoff (MK) technique is shown to be substationally more accurate than ordinary Maslov integration when pseudo-caustics are present. Furthermore, it is more robust and automated than the phase-partitioning technique in curing the problem of joint caustics and pseudo-caustics. We also show that the MK scheme can be more efficient than other Kirchhoff modelling techniques where the kernel of integration is obtained by GRT.

Key words: caustics, geometric ray theory, Kirchhoff theorem, Maslov asymptotic theory, pseudo-caustics, seismic waveforms.

1 INTRODUCTION

Ray-based techniques for waveform modelling are attractive in seismic data intepretation because they provide insight into how a wave front will respond to a given velocity structure. The user has the luxury of being able to monitor a given phase in isolation as it steps through the medium. Zeroth-order asymptotic ray theory (ART), or alternatively geometric ray theory (GRT) is concerned with only the relatively high-frequency component of the waveform, provided the ray tube does not vanish. However, in complex media, lower-frequency waveform distortion will be common, and ray tubes shrink to zero at places called caustics. Other asymptotic techniques take steps to handle these finite-frequency effects. For generally inhomogeneous media they are, for instance, Maslov asymptotic theory (Chapman & Drummond 1982), Gaussian beam summation (Červený, Popov & Pšenčík 1982) and the coherent-state transformation (Klauder 1987; Foster & Huang 1991). These techniques include the wavefield contributions of neighbouring or non-geometrical rays at a receiver. As a result they can predict signals in shadow regions where there are no geometric arrivals and, unlike GRT, they are valid in regions at and near caustics. In this paper we present a Maslov–Kirchhoff hybrid technique.

In an accompanying paper (Huang *et al.* 1998, hereafter HM1) we assess the accuracy of Maslov asymptotic theory

(MAT) through comparisons with waveforms synthesized using finite-difference methods. It was shown that Maslov waveforms are reasonably accurate at high frequencies. As discussed in HM1, the occurrence of pseudo-caustics (Kendall & Thomson 1993) hinders the implementation of automated simple-to-use techniques for generating Maslov waveforms.

Another group of techniques for waveform modelling is known as the Kirchhoff method. In this approach the wavefield is represented as an integral over one or more intermediate surfaces (Haddon & Buchen 1981; Frazer & Sinton 1984). As with the Maslov method, it is the aim of Kirchhoff methods to include, via the integration, the contributions of neighbouring rays to generate lower-frequency wave components. The kernel of this integrand is commonly obtained using ART, where rays are traced from the source and receiver positions to the intermediate surface. However, the technique is only valid if the rays do not pass through caustics on the intermediate surface, or more intermediate surfaces are needed, which, in practice, can be a severe limitation.

In this paper we introduce a technique for calculating waveforms using the Maslov method coupled with a Kirchhoff integration. The kernel of the Kirchhoff integral is constructed using the Maslov method, which, unlike ART, is valid in the vicinity of ray focusing and caustics. Pseudo-caustics will still arise in the Maslov summation, but the Kirchhoff integration over secondary sources has the effect of mitigating the spurious signals associated with pseudo-caustics. In essence, we boost the real signal and suppress the numerical 'noise' associated with the pseudo-caustics. It is through the combined application of the Maslov and Kirchhoff integrals that we can take advantage of each technique's strengths and, at the same time, overcome some of their limitations.

2 THEORY

Both Maslov asymptotic theory and Kirchhoff methods have been presented separately in many papers. For a review of the Maslov method the reader is referred to Chapman & Drummond (1982), Thomson & Chapman (1985), Kendall & Thomson (1993), Brown (1994), Liu & Tromp (1996), Huang & West (1997) and HM1. A review of the Kirchhoff integral can be found in Haddon & Buchen (1981), Frazer & Sinton (1984), Zhu (1988), Berkhout & Wapenaar (1989) and Wapenaar *et al.* (1989). In this paper we introduce the necessary formalism for combining the Maslov and Kirchhoff methods. For simplicity, equations (and later computations) are given only for the 2-D acoustic case where the density is assumed constant. More complicated cases such as 3-D elastic wave propagation can be treated in an exactly parallel manner.

In the frequency (ω) domain, the GRT solution Φ to the inhomogeneous Helmholtz equation $(\partial^2_{x_1}+\partial^2_{x_3}+(\omega/c)^2)\Phi = -4\pi\delta(x_{s1})\delta(x_{s3})$ at a receiver point $\mathbf{x}_r=(x_{r1}, x_{r3})$ in a 2-D (x_1, x_3) acoustic medium in which $c(\mathbf{x})$ is the velocity is (e.g. Hudson 1980 and Frazer & Sinton 1984)

$$\Phi^{\mathrm{GRT}}(\omega, \mathbf{x}_r) = \sum_{\text{rays}} \frac{2^{1/2}c(\mathbf{x}_r)}{|J(\mathbf{x}_r)|^{1/2}} \left(\frac{\pi}{-i\omega}\right)^{1/2} \exp[-i\mathrm{sgn}(\omega)\pi\sigma/2] \times \exp[i\omega T(\mathbf{x}_r)], \quad (1)$$

where the subscripts s and r refer to the source and receiver, respectively, and σ is the KMAH index, which monitors ray passage through each caustic (e.g. Chapman & Drummond 1982 and Brown 1994). The summation Σ is over all rays that arrive at the receiver $\mathbf{x}_r$. The GRT amplitude is inversely proportional to the square root of the Jacobian $J(\mathbf{x}_r)=\partial\mathbf{x}/\partial\boldsymbol{\nu} = \partial(x_1, x_3)/\partial(T, q)$, where $\boldsymbol{\nu}=(T, q)$ represents the ray coordinate system consisting of the traveltime T and the initial take-off angle q. This Jacobian can be thought of as the cross-sectional area of the ray tube (Chapman & Drummond 1982). It is well known that the GRT approximation (1) breaks down at caustics, regions where rays focus and J vanishes, and provides no information about the wavefield energy which arrives in geometrically shadowed regions (Chapman 1985).

In order to model waveforms in such regions of interest, Maslov (1965, 1972) suggested an integral transform solution which amounts to ray summation over the receiver neighbouring rays. It is a solution to the Helmholtz equation in the spatial Fourier transform domain. For the sake of illustration, we have here assumed the transform domain, a mixed geometrical space and slowness space, to be (x_1, p_3). The Maslov integral (MI) is then

$$\Phi^{\mathrm{MI}}(\omega, \mathbf{x}_r; \mathbf{x}_s) = i\int \frac{c(p_{s3})}{|\tilde{J}(p_{s3})|^{1/2}} \exp(-i\pi\tilde{\sigma}/2) \times \exp[i\omega\tilde{\theta}(\mathbf{x}_r, p_{s3})]dp_{s3}, \quad (2)$$

where $\tilde{\sigma}$ is the Maslov index, which functions to ensure the continuity of a physical waveform across a pseudo-caustic by changing its value by one whenever such a point is passed (e.g. Kendall & Thomson 1993; Brown 1994). The term $\tilde{J}$ is the Maslov Jacobian which is related to the (GRT) Jacobian by the canonical transformation $\tilde{J}(p_{s3}) = (\partial p_{s3}/\partial p_{r3})(\partial p_{s3}/\partial x_{r3})J(p_{s3})$. See Chapman & Drummond (1982) and Thomson & Chapman (1985) for details.

When rays pass through a caustic and focus in the spatial (x_1, x_3) domain, they will not cross in the transform (x_1, p_3) domain (Liouville's Theorem; Thomson & Chapman 1985). It is by virtue of this fact that the Maslov amplitude is stable at caustics. On the other hand, the Maslov integral (2) is inaccurate at pseudo-caustics, places where rays are parallel in the spatial domain but focus in the transform domain (Frazer & Phinney 1980; Chapman & Drummond 1982; Kendall & Thomson 1993; Brown 1994). Kendall & Thomson (1993) proposed a 'phase-partitioning' technique for treating pseudo-caustic problems, and in HM1 it was shown that this technique gives accurate results when it is applicable. The downside is that it is not easily automated, as it requires intermediate input from an informed user.

It should be noted that the Maslov integral presented here is slightly different from that presented in HM1. Here the integration is over the source slowness p_{s3}, whereas in HM1 the integration is over the receiver slowness. In cases of pseudo-caustics, integration over receiver slowness is singular as there will not be a unique slowness for each ray. On the other hand, integration over source slowness is not singular, and is computationally convenient because each ray is uniquely defined by a source slowness (or take-off angle), even in the presence of pseudo-caustics. Nevertheless, integration through pseudo-caustics still gives rise to erroneous low-frequency contributions to the waveform (Frazer & Phinney 1980; Brown 1994).

According to Liouville's theorem (Maslov & Fedoriuk 1981; Thomson & Chapman 1985), caustics and pseudo-caustics will never occur at the same location. Maslov (1965, 1972) therefore

proposed a globally valid high-frequency wavefield solution by appropriate blending of the GRT and MI solution components, i.e. (1) and (2). Although blending provides an efficient tool for modelling waveforms in regions where caustics and pseudo-caustics are well separated compared with the dominant wavelength (Brown 1994; Liu & Tromp 1996; Huang & West 1997), it fails in practice at places where caustics and pseudo-caustics occur in close proximity to each other (Kendall & Thomson 1993). We refer to these as *joint caustics*. Such a situation is not uncommon when treating arbitrary 2-D or 3-D geological structure (Kendall & Thomson 1993). Clearly a different approach is required.

Unlike real caustics, pseudo-caustics are mathematical artefacts which are not expressed in the real physical waveform. It therefore seems reasonable to try to suppress the pseudo-caustic signatures through summing many Maslov waveforms from a series of secondary or virtual sources in a Kirchhoff integration. Each secondary-source Maslov waveform may contain some pseudo-caustic signals, but the errors will be, in general, randomly distributed. They then will cancel during the summation.

Kirchhoff integration invokes Huygens' principle that an intermediate wavefield can be treated as a series of secondary sources so the final wavefield is a superposition of the wave components of these secondary sources (Berkhout & Wapenaar 1989; Wapenaar *et al.* 1989). Let $\Phi(\omega, \mathbf{x}_k; \mathbf{x}_s)$ be the intermediate wavefield from the primary source to the Kirchhoff integration line (KIL) $\mathbf{x}_k$ (a plane in three dimensions), and $\Phi(\omega, \mathbf{x}_r; \mathbf{x}_k)$ be the secondary wavefields from the secondary sources on the KIL to the receiver. The Kirchhoff integral (Rayleigh-type) gives the real wavefield at the receiver point:

$$\Phi(\omega, \mathbf{x}_r; \mathbf{x}_s) = -2 \int \partial_{x_{k1}} \Phi(\omega, \mathbf{x}_r; \mathbf{x}_k) \Phi(\omega, \mathbf{x}_k; \mathbf{x}_s)\, dx_{k3}\,. \tag{3}$$

Note that all the intermediate and secondary waveforms are calculated using the MI solution (2) at a low cost. Pseudo-caustics can arise but they do not impede the calculation. The normal derivative of the secondary waveform in (3) is given by its Maslov form,

$$\partial_{x_{k1}} \Phi^{MI}(\omega, \mathbf{x}_r; \mathbf{x}_k) \simeq -\omega \int \frac{c(p_{k3}) p_{k1}(p_{k3})}{|\tilde{J}(p_{k3})|^{1/2}} \exp(-i\pi\tilde{\sigma}/2) \times \exp[i\omega\tilde{\theta}(\mathbf{x}_r, p_{k3})]\, dp_{k3}\,. \tag{4}$$

This integral is easily evaluated. The time-consuming step is tracing rays from the primary source to the intermediate KIL and then tracing rays from the secondary sources on the KIL to the Maslov integration line through the receiver.

3 IMPLEMENTATION

The Maslov–Kirchhoff (MK) method is schematically illustrated in Fig. 1. To model the wavefield propagating from a (primary) source (star) to a line of receivers (solid circles), a Kirchhoff integration line is introduced somewhere between the source point and the receiver line. The modelling is completed in three steps: first we calculate Maslov waveforms at the seondary sources on the intermediate KIL using the KIL as the Maslov integration axis; then we compute the Maslov waveforms at the receiver line from each secondary source; and finally we sum all the Maslov waveforms from the secondary sources in the Kirchhoff integral (3). Any pseudo-caustic signals arising in the first two steps will tend to cancel in the third step. The reader is referred to HM1 for details of the ray tracing and Maslov integration employed in our numerical calculations. The Kirchhoff integration is performed using a simple trapezoidal rule numerical integration scheme.

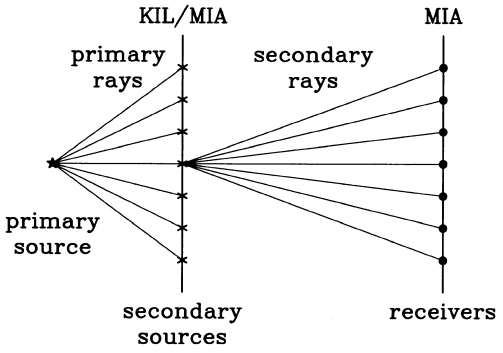

Figure 1. Geometry of the Maslov–Kirchhoff seismogram for a point source, where an intermediate KIL/MIA (Kirchhoff integration line/Maslov integration axis) is introduced between the primary source (star) and the final receivers (solid circles). Primary rays are traced from the primary source to KIL/MIA, and secondary rays from the secondary sources to the final MIA. The point-source responses on the KIL/MIA and MIA are all obtained by MI (the pure Maslov integral solution).

To assess the accuracy of our technique we have compared the Maslov–Kirchhoff waveforms with those predicted using the finite-difference (FD) and phase-partitioning Maslov integral (PPMI; Kendall & Thomson 1993) schemes in a variety of cases. Again the reader is referred to HM1 for details of the two schemes.

4 EXPERIMENT

To demonstrate the MK method's effectiveness we examine 2-D acoustic wave propagation through a circular low-velocity Gaussian perturbation in an otherwise uniform-velocity medium, where the density is everywhere constant (this is due to a limitation in the FD code we used, not a limitation in the MK technique). As shown in Fig. 2, the perturbation acts as a converging lens and produces the familiar butterfly wave front (triplication) with cusps and ray caustics where the waveforms are distorted and stronger. Wave-front inflexions also arise, where rays become parallel and pseudo-caustics occur.

4.1 Geometrical problems of the wavefield

The test example is also a good example of joint caustics, so it is hard to compute accurate synthetic seismograms using GRT or the Maslov method, if one tries to do the calculation in a single step. Fig. 3 displays ray traveltimes and amplitudes in the space and slowness domains, with the left-hand column displayed as a function of receiver position and the right-hand column a function of receiver slowness. Both GRT and MI amplitudes have singularities at almost the same locations.

Changing the Maslov variable to source slowness can make the Maslov integral integrable (although not necessarily accurate). This is illustrated in Fig. 4. The geometrical problems arising in the receiver slowness domain are depicted in the left column. These are the cusps C'_x and C''_x and inflections C'_p and C''_p (on the forward branches) of the traveltime (a); inflections

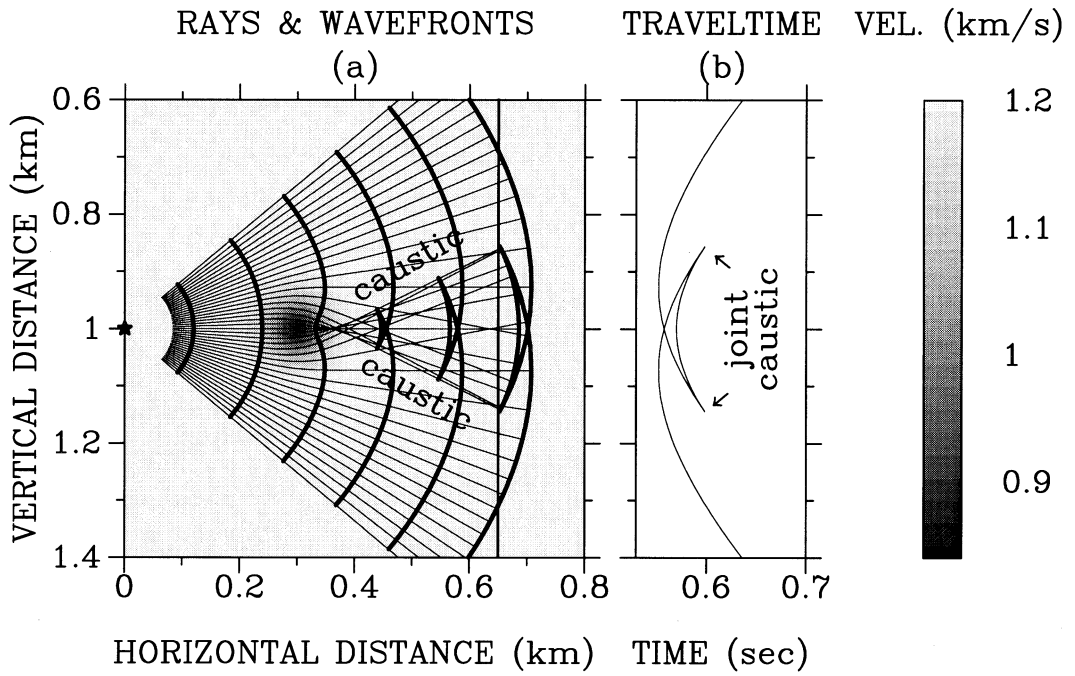

Figure 2. (a) A 2-D acoustic velocity model with homogeneous background, which is perturbed by a circular velocity reduction (up to 30 per cent). The relative velocity anomaly is described by a circular Gaussian function centred at (0.3, 1.0) i.e. $-0.3\exp\{-[(x_1-0.3)^2+(x_3-1.0)^2]/0.05^2\}$. Rays (thin lines) and wave fronts (thick lines) are shot from a point source at (0, 1). Note the caustic lines and wave-front triplications in the wavefield. (b) The traveltime curve recorded on the receiver line at $x_1 = 0.65$ km.

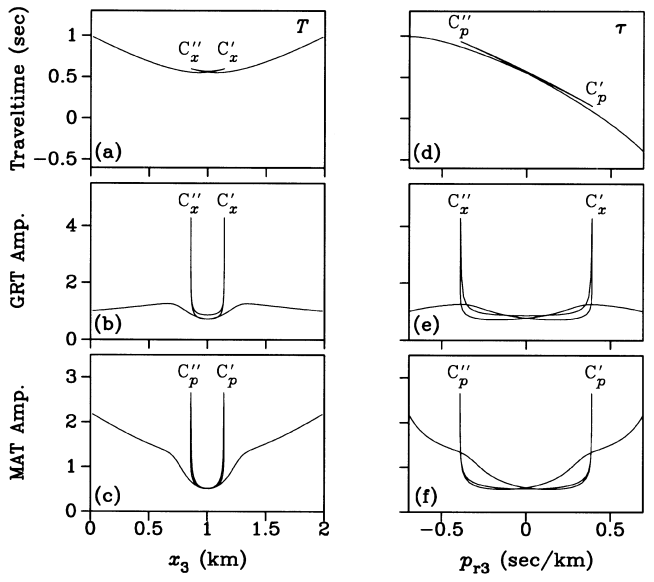

Figure 3. Ray traveltimes and amplitudes in space and slowness domains for the model in Fig. 2: an example of joint caustics. The upper panel shows the ray traveltimes, one in space domain T folding at caustics (C'_x and C''_x) and the other in receiver slowness domain τ (i.e. the intercept time) folding at pseudo-caustics (C'_p and C''_p); the middle panel shows the GRT amplitude, which is singular at caustics (C'_x and C''_x); the lower panel shows MAT amplitude, which is singular at pseudo-caustics (C'_p and C''_p). Data are plotted in the space domain on the left and in the receiver slowness domain on the right. At this plotting scale, the positions of caustics and pseudo-caustic singularities are indistinguishable.

C'_x (on the reversed branch) and C''_x and cusps C'_p and C''_p of the intercept time τ (b); multi-evaluation of the phase function $\tilde{\theta}$ (e.g. for receiver at $x_3 = 1$ km) (c); and multi-evaluation and singularity of the amplitude (d).

As shown on the right side of Fig. 4, all the above functions become single-valued in the new source slowness domain (p_{s3}). This is shown by the traveltime in (f), the intercept time in (g), the phase function in (h) and the normalized MAT amplitude in (i). [In particular, the caustics (cusps) of the traveltime in (a) change to the stationarities C'_x and C''_x in (f). The pseudo-caustics (cusps) of the intercept time in (b) change to the stationarities in (g).] The new Maslov amplitude is everywhere finite (i). However, the non-physical stationarities of the phase function (h) resulting from the pseudo-caustics (marked by the dashed lines) still causes appreciable error in the MI seismogram (Frazer & Phinney 1980; Brown 1994) as will be shown in Fig. 5(a).

4.2 Kirchhoff summation, error reduction and optimum sampling

The effect of Kirchhoff summation in reducing the pseudo-caustic errors of a one-step MI calculation is shown in the various panels of Fig. 5. For comparison purposes, Zeng's (1996) explicit 2-D fourth-order FD software has been employed to compute the true wavefield (solid lines in all panels). To accommodate the frequency limits of the FD solution, the wavefield has been band limited at a relatively low dominant frequency (about 45 Hz). Thus, it propagates paths of about 25 dominant wavelengths and diffracts smoothly from the cusp into the shadow zone.

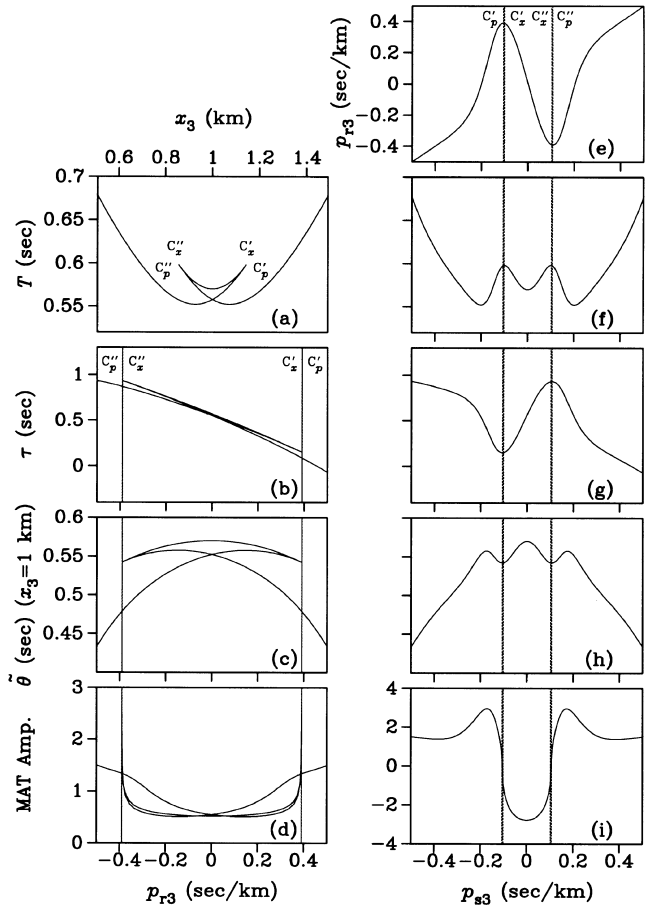

Figure 4. Showing that MI singularities at pseudo-caustics are removed by switching from source to receiver slowness domain. The left and right columns show MI asymptotic data for the model in Fig. 2 in receiver and source slowness, respectively. Note the lack of singularities or cusps in the source-slowness data. Parts (a) and (f), (b) and (g), (c) and (h), (d) and (i) are, respectively, graphs of traveltime T, intercept time τ, Maslov phase $\tilde{\theta}$ and Maslov amplitude. Part (e) shows the relationship between receiver and source slowness. In the source slowness domain the pseudo-caustics manifest themselves as local minima in the $\tilde{\theta}$-function which lead to erroneous waveform contributions.

Fig. 5(a) shows the pseudo-caustic error of the one-step calculation. Artefacts consisting of two linear phases nearly tangent to the two cusps are present. The two-step MK results are displayed in (b), (c), (d) and (f). All are modelled by extrapolating an unfolded intermediate wavefield from a KIL of length 0.5 km at $x_1 = 0.2$ km. The first three have a sufficiently small time sampling step (0.2 ms), but different numbers of intermediate wavefield traces have been input into the Kirchhoff summation: 26 for (b), 51 for (c) and 101 for (d), which correspond to different sampling rates of traces per dominant wavelength: 1.5 for (b), 3 for (c) and 6 for (d). The last two give satisfactory results. Fig. 5(e) shows [using the same sampling parameters as (d)] the result of using GRT as the kernel of the Kirchhoff integral. Comparison between the results by MK and MI demonstrates that the pseudo-caustic errors present in (a) have been satisfactorily reduced in all the Kirchhoff summations. The late spurious oscillations in (b) are due to coarse discretization of the Kirchhoff integral, but can be easily suppressed by adding more traces into the summation, as shown in (c), (d) and (f). The results in (c) and (d) are satisfactory. A sampling rate of at least three traces per dominant wavelength is suggested from this test.

Fig. 5(f) shows that systematic error arises if the time sampling is made too coarse. A visible timing error appears in several places and some subtle waveform features are not accurately resolved; the waveform at depth 1 km is one such example. We see that MK does require a finer time sampling rate than one-step MI (or GRT). In these tests MI needs at least 20 points per wavelet but MK at least 40. (Note that a sampling rate of 15 points per wavelet can only ensure accuracy of traveltime, not waveform.)

It is interesting to compare MK and RK [the ray-Kirchhoff seismogram method in which GRT serves as the kernel of the interpretation (Haddon & Buchen 1981)]. The wavefield modelled by RK through the same intermediate wavefield as in Fig. 5(c) is given in (e). We see that RK does produce cusp diffractions, but the waveforms of the late branch contain errors, and a more serious error appears at a depth of 0.88 km (behind the later branch). These errors are caused by the caustics of the secondary-source rayfields. Their elimination requires many more Kirchhoff integration steps and substantially more computation time.

The computational efficiency of one-step MI is extremely high. MK needs more computation time than MI by tracing more rays from secondary sources to the receiver line; the time required depends on the number of secondary sources and is often one order of magnitude larger. Nevertheless, MK maintains a high computational efficiency compared with FD. In these computations, the times that MI, MK and FD need on a SUN SPARCstation 10 can be optimized to 14 s, 5 min and 30 min, respectively.

The whole purpose of asymptotic methods is to model seismograms at the relatively high frequencies often employed in seismology (propagation paths $\approx 10^2$ dominant wavelengths). Thus, the above test on MK has been repeated for frequencies five times higher and propagation paths of more than 125 dominant wavelengths. Results are given in the left column of Fig. 6. Note that because the traveltime contains pseudo-caustics only on the forward branches, PPMI is applicable and has been employed to compute the true wavefield (solid lines). (FD would spend days of computation time on a SUN SPARCstation 10, provided the memory is sufficient.) In (a) we see that the MI seismogram has been degraded by a pair of linear pseudo-caustic phases. Interestingly, the error level is similar in amplitude to that in the previous low-frequency case, although more localized in time. Fig. 6(b) shows the MK seismogram computed using 231 secondary sources with a spacing of 2 m at the same KIL position as before ($x_1 = 0.2$ km) during a time period of tens of minutes. As shown in (b), the MK result still contains some local errors between depths of 0.90 and 0.96 km but it is much more acceptable than that by ML. The diffraction event modelled by MK at a depth of 0.8 km has become slightly inconsistent with that predicted by PPMI, but this is of little importance because the event is becoming weak at this distance from the cusp.

In both the high- and low-frequency wavefield modellings, errors appear at similar positions in the MK seismograms (between depths of 0.90 and 0.96 km). In order to track their origin, the wavefields of individual secondary sources have

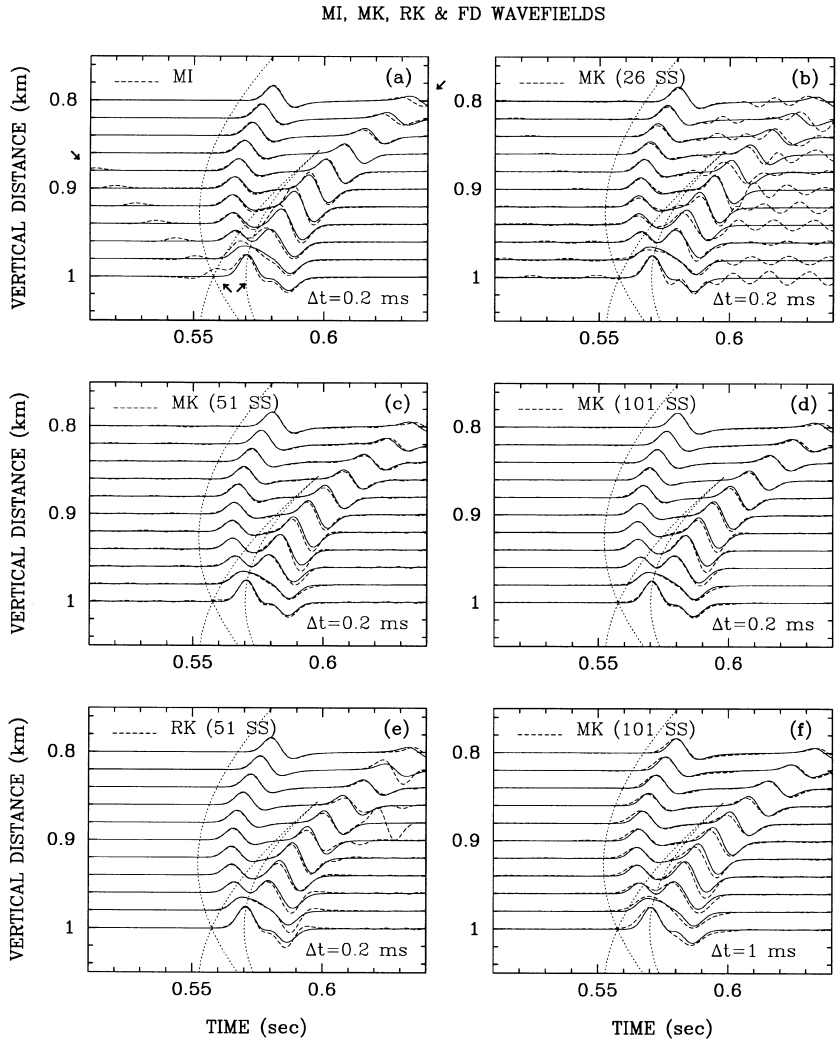

Figure 5. Maslov integral (MI), Maslov–Kirchhoff (MK) and ray-based-Kirchhoff (RK) wavefields (dashed lines) at the receiver line (RL) $x_1 = 0.65$ km, compared with the FD results (solid lines). (a) shows the erroneous pseudo-caustic signals with linear moveout across the section produced by one-step MI (pseudo-caustic phases marked by arrows). Parts (b), (c) and (d) show MK wavefield with fine time sampling (0.2 ms) for 26, 51 and 101 secondary sources (SS). (e) RK wavefield for the same case as in (c). (f) MK wavefield with a longer time sampling interval (1 ms).

been examined. Examples are displayed in the right column of Fig. 6. The secondary sources are located at depths 0.932, 0.960 and 0.988 km. We see that pseudo-caustic errors are generated for each of the secondary sources and although most are at different locations, some of them actually focus. The focal point in (c) is different from the true events. (d) shows that the summation of individual wavefields can easily reduce the pseudo-caustic errors provided they do not focus. If focusing does occur the errors remain no matter how many secondary sources are used and they tend to occur as isolated events.

4.3 Tolerance of the intermediate KIL position

To test the tolerance of the intermediate KIL position, two different KIL positions are investigated, one close to the source at a distance $x_1 = 0.1$ km and the other in the central region but across the folded wavefield at $x_1 = 0.4$ km. The resulting seismograms are shown in Fig. 7. (Note the dominant frequency is the same as shown in Fig. 5.) The intermediate wavefield close to the source is simple. The MK seismogram using 81 traces 5 m apart of this intermediate wavefield is shown in (a). Two pseudo-caustic phases still exist, one crossing the window from the lower-left corner to the upper-right corner, and the other simply its mirror image. In this case, MK provides little improvement over MI. Interestingly, the spurious pseudo-caustic phases shift in time.

Unlike the previous cases, the intermediate wavefield (computed by MI) at the second KIL position ($x_1 = 0.4$ km) contains pseudo-caustic errors (Fig. 7b); testing the MK effect seems more attractive. The result from 81 traces is given in Fig. 7(c). Comparison with FD shows that the MK results contain only minor errors and are free from the effect of the intermediate pseudo-caustic errors. Note that the weak spurious arrivals between the direct and the diffracted waves, which are marked by an arrow, are due to the cut-off of the Kirchhoff integral. They could be easily remedied by tapering the cut-off, for example by weighting the secondary-source strength distribution with a Gaussian function.

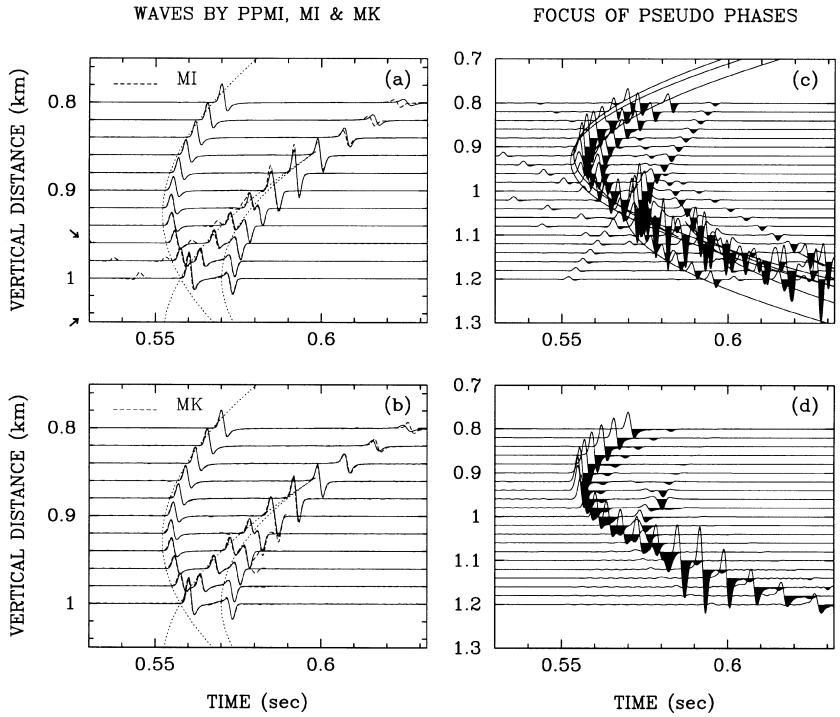

Figure 6. Left column: high-frequency wavefields at the receiver line $x_1 = 0.65$ km modelled by MI (dashed lines in a) and MK (dashed lines in b), compared with the accurate PPMI (all solid lines). Linear pseudo-caustic errors in (a) (marked by arrows) have been mostly suppressed in (b) except for the small region between depths of 0.90 and 0.96 km. The diffraction at 0.82 km has been improved. Right column: (c) the focusing of pseudo-caustic phases in the wavefield contributions from three individual secondary sources and (d) their summation. The sources lie at depths of 0.932, 0.960 and 0.988 km. Because the pseudo-caustic phases have a focus that is away from real signals [near the point (0.58, 0.94)], the errors remaining in (d) are still quite prominent between 0.92 and 1.2 km and $t = 0.58$ s, although much weaker than in a direct MI calculation.

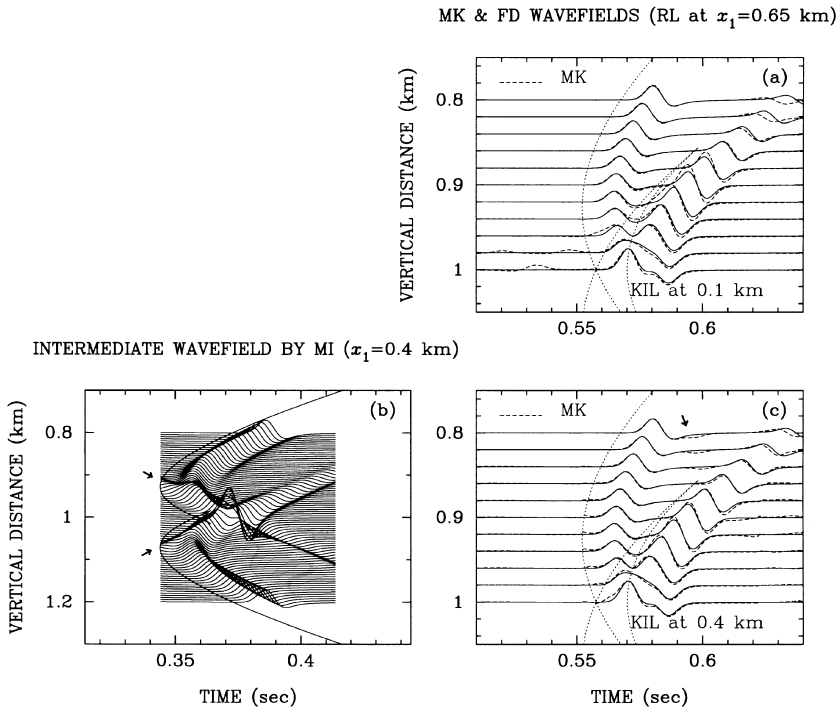

Figure 7. Wavefields modelled by MK (dashed lines) via different KIL positions, and compared with the accurate FD result (solid lines in a and c). For (a) the KIL is 0.1 km from the source; for (c) it is in the central region at $x_1 = 0.4$ km. In (a) the pseudo-caustic errors have only been shifted away from the real waveform; however in (c) they have been very satisfactorily suppressed, although some of the intermediate wavefields contain large pseudo-caustics errors (i.e. those marked by arrows in b).

5 CONCLUSIONS

A hybrid Maslov–Kirchhoff modelling method has been presented in this paper. It has been shown that the use of intermediate virtual sources tends to randomize pseudo-caustic signals in the Maslov waveforms so they really are reduced in the Kirchhoff summation. Incoherent pseudo-caustic errors can be easily suppressed by the use of a few secondary sources but more are required to maintain the accuracy of the Kirchhoff integral. A sampling rate of at least three traces per dominant wavelength was required in the example.

Some care must be taken in choosing the size and location of a Kirchhoff integration line. It was found that this line or surface should be extended to include all virtual sources which emit wave fronts arriving at the receiver line within the time window of interest. An additional zone of the size of a dominant wavelength is preferable if cut-off tapering is wanted. The integration line or surface should be placed roughly centrally between the source and the receiver such that the pseudo-caustic signals can be significantly randomized. Often one such line or surface is sufficient regardless of the number and positions of medium anomalies (Huang, Liu & West 1996).

The proposed modelling method has been shown to be more accurate than ordinary Maslov integration when pseudo-caustics are present. Furthermore, the technique is more robust and automated than Kendall & Thomson's (1993) phase-partitioning technique in curing the joint-caustic problem. Although it may require one order of magnitude larger computation time than ordinary Maslov integration, it is still several times faster than finite-difference methods. In many applications concerning high-frequency wave propagation, FD can be prohibitively expensive, whereas the new technique can be easily implemented on a common workstation. Compared with other Kirchhoff modelling techniques, the new technique is more efficient than Haddon & Buchen's (1981) ray-Kirchhoff method, because a single KIL has been shown to be sufficient to remove most pseudo-caustic errors. This technique has been applied to modelling complex cross-well wave propagation (Huang *et al*. 1996), but further work is needed to explore its utility in three dimensions.

ACKNOWLEDGMENTS

Prof. C. J. Thomson is thanked for helpful discussions. Dr X. Zeng is thanked for providing his FD software. Constructive reviews by Michael Weber and an anonymous reviewer are gratefully appreciated. The research was supported by an E. F. Burton fellowship in the Department of Physics, University of Toronto, to XH, and NSERC funding to GRW.

REFERENCES

Berkhout, A.J. & Wapenaar, C.P.A., 1989. One-way versions of the Kirchhoff integral, *Geophysics,* **54,** 460–467.

Brown, M.G., 1994. A Maslov–Chapman wavefield representation for wide-angle one-way propagation, *Geophys. J. Int.,* **116,** 513–526.

Červený, V., Popov, M.M. & Pšenčík, I., 1982. Computation of wave fields in inhomogeneous media—Gaussian beam approach, *Geophys. J. R. astr. Soc.,* **70,** 109–128.

Chapman, C.H., 1985. Ray theory and its extensions: WKBJ and Maslov seismograms, *J. Geophys.,* **58,** 27–43.

Chapman, C.H. & Drummond, R., 1982. Body-wave seismograms in inhomogeneous media using Maslov asymptotic theory, *Bull. seism. Soc. Am.,* **72,** S227–S317.

Foster, D.J. & Huang, J.-I., 1991. Global asymptotic solutions of the wave equation, *Geophys. J. Int.,* **105,** 163–171.

Frazer, L.N. & Phinney, R.A., 1980. The theory of finite frequency body wave synthetic seismograms in inhomogeneous elastic media, *Geophys. J. R. astr. Soc.,* **63,** 691–717.

Frazer, L.N. & Sinton, J.B., 1984. A Kirchhoff method for the computation of finite-frequency body wave synthetic seismograms in laterally inhomogeneous media, *Geophys. J. R. astr. Soc.,* **78,** 413–429.

Haddon, R.A.W. & Buchen, P.W., 1981. Use of Kirchhoff's formula for body wave calculations in the Earth, *Geophys. J. R. astr. Soc.,* **67,** 587–598.

Huang, X., 1997. Contributions to seismogram modeling by classical Maslov and new Maslov-Kirchhoff methods, *PhD thesis,* University of Toronto, Canada.

Huang, X. & West, G.F., 1997. Effects of weighting functions on Maslov uniform seismograms: a robust weighting method, *Bull. seism. Soc. Am.,* **87,** 164–173.

Huang, X., Liu, W. & West, G.F., 1996. Efficient modeling of primary waves in a complicated medium by the Maslov-Kirchhoff seismogram method, *66th Ann. Int. Mtg, Soc. Expl. Geophys.,* Expanded Abstracts, 283–286.

Huang, X., Kendall, J.-M., Thomson, C.J. & West, G.F., 1998. A comparison of the Maslov integral seismogram and the finite-difference method, *Geophys. J. Int.,* **132,** 584–594 (this issue).

Hudson, J.A., 1980. *The Excitation and Propagation of Elastic Waves,* Cambridge University Press, Cambridge.

Kendall, J.-M. & Thomson, C.J., 1993. Maslov ray summation, pseudo-caustics, Lagrangian equivalence and transient seismic waveforms, *Geophys. J. Int.,* **113,** 186–214.

Klauder, J.R., 1987. Semiclassical quantization of classically chaotic systems, *Phys. Rev. Lett.,* 59, 748–750.

Liu, X. & Tromp, J., 1996. Uniformly valid body-wave ray theory, *Geophys. J. Int.,* **127,** 461–491.

Maslov, V.P., 1965. *Theory of Perturbations and Asymptotic Methods* Izd., MGU, Moscow (in Russian).

Maslov, V.P., 1972. *Théorie des Perturbations et Méthodes Asymptotiques,* Dunod, Paris.

Maslov, V.P. & Fedoriuk, M.V., 1981. *Semi-Classical Approximation in Quantum Mechanics*, D. Reidel, Dordrecht, the Netherlands.

Thomson, C.J. & Chapman, C.H., 1985. An introduction to Maslov's asymptotic method, *Geophys. J. R. astr. Soc.,* **83,** 143–168.

Wapenaar, C.P.A., Peels, G.L., Budejicky, V. & Berkhout, A.J., 1989. Inverse extrapolation of primary seismic waves, *Geophysics,* **54,** 853–863.

Zeng, X., 1996. Finite difference modeling of viscoelastic wave propagation in a generally heterogeneous medium in the time domain, and a dissection method in the frequency domain, *PhD thesis,* University of Toronto, Canada.

Zhu, T., 1988. A ray-Kirchhoff method for body-wave calculations in inhomogeneous media: theory, *Geophys. J.,* **92,** 181–193.